Analytical solutions to the electromagnetic field in a cylindrical shell excited by external axial current*

Wu Jing(吴 静)† and Xiao Chun-Yan(肖春燕)

School of Automation Science and Electrical Engineering, Beihang University, Beijing 100191, *China*

(Received 11 September 2009; revised manuscript received 9 November 2009)

The solutions to the electromagnetic field excited by a long axial current outside a conductive and magnetic cylindrical shell of finite length are studied in this paper. The more accurate analytical solutions are obtained by solving the proper boundary value problems by the separation variable method. Then the solutions are simplified according to asymptotic formulas of Bessel functions. Compared with the accurate solutions, the simplified solutions do not contain the Bessel functions and the inverse operation of the singular matrix, and can be calculated out fast by computers. The simplified solutions are more suitable for the cylindrical shell of high permeability and conductivity excited by a high frequency source. Both of the numerical results and the physical experimental results validate the simplified solutions obtained.

Keywords: analytical solution, electromagnetic field, ferrite shell, axial current
PACC: 4110F, 7550B

1. Introduction

In the electronic and electrical engineering fields, the cylindrical shell-shaped ferrite cores or iron cores of finite length are widely used in inductors, current transformers, magnetic amplifiers and relays. These cores are made of sintered magnetic and conductive powder or thin sheets. When they are positioned beside the cables or transmission lines, the electromagnetic field in core will be interfered, which can reduce the accuracy of the devices and increase the eddy current losses. To shield effectively the magnetic field interference and calculate accurately the eddy losses it is necessary to analyse the electromagnetic field in the cores excited by other sources.

Unlike those rotational and symmetrical fields such as the fields in an infinite layered space or infinite length cylinder or cylindrical shell, which can be regarded as two-dimensional (2D) fields,[1−4] the fields in the cylindrical ferrite shell of finite length are usually three-dimensional (3D) and it is difficult to obtain completely accurate analytical solutions. Approximate analytical solutions to the fields excited by the long axial current in the finite length conductive cylindrical shell,[5,6] by the short radial current centred in the shell,[7] by the toroidal coils around the shell,[8] by the long radial cable outside the conductive cylinder,[9] by the symmetrical coils around the magnetic and conductive cylinder,[10] by the current injected into a surface of a conductor which is equivalent to a cylinder with infinite thickness,[11] or by coaxially placed electrodes in a metal cylindrical specimen[12] were obtained. Furthermore, for some very complex models such as a ferrite-cored coil over a layered conducting half-space[13] and an arbitrarily shaped coil in the mouth of a cylindrical borehole,[14] approximate analytical expressions on the fields could also be obtained by solving proper boundary problems. To solve the above three-dimensional fields, the most important point is to determine boundary conditions. Two special boundary conditions were usually used.[15] One is that the normal component of electric field strength near the surface of a good conductor equals zero, and the other is that the normal component of magnetic field strength near the surface of a good magnetic medium equals zero.

The fields excited by the axial current outside the finite length cylindrical shell are discussed in this paper. Firstly, more accurate and complex analytical solutions are derived. Then, the analytical solutions are simplified so that they are more suitable for cylindrical shell having large size and high conductivity and permeability. Finally, the accurate solutions and the simplified solutions are compared, and physical experiments are demonstrated to validate the solutions.

*Project supported by the State Key Lab of Power Systems, China (Grant No. SKLD09KM06).
†Corresponding author. E-mail: wujing06@buaa.edu.cn
© 2010 Chinese Physical Society and IOP Publishing Ltd

2. Analytical solutions

2.1. Constraint equations

The cylindrical ferrite shell interfered by an external long axial current is modelled as shown in Fig. 1. The cylindrical shell is assumed to be a uniform, isotropic and linear medium. Its conductivity is γ, the magnetic permeability is μ (the relative permeability is $\mu_{\rm r}$) and the permittivity is ε. The axial current varies with time t in the form of $I\,{\rm e}^{{\rm i}\omega t}$, $\omega = 2\pi f$ and f is the frequency. In the cylindrical shell, the constraint equations are

$$\nabla^2 \boldsymbol{E} + k^2 \boldsymbol{E} = 0, \tag{1}$$

$$\boldsymbol{\nabla} \cdot \boldsymbol{E} = 0, \tag{2}$$

where $\boldsymbol{E}$ is the electric field strength and $k^2 = \omega\mu(\omega\varepsilon - {\rm i}\gamma)$. $\boldsymbol{E}$ is symmetrical along z: $E_\rho(\rho,\phi,-z) = E_\rho(\rho,\phi,z)$, $E_\phi(\rho,\phi,-z) = -E_\phi(\rho,\phi,z)$ and $E_z(\rho,\phi,-z) = E_z(\rho,\phi,z)$. The magnetic induction strength is $\boldsymbol{B} = [-(\boldsymbol{\nabla}\times\boldsymbol{E})/({\rm i}\omega)]$ and the magnetic field strength is $\boldsymbol{H} = \boldsymbol{B}/\mu_0$.

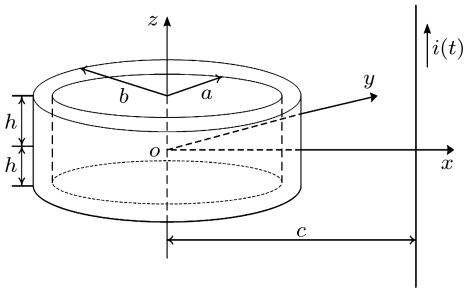


Fig. 1. Physical model of the cylindrical shell excited by the external axial current.

In air, the constraint equations are

$$\nabla^2 \boldsymbol{E}' + k_0^2 \boldsymbol{E}' = {\rm i}\omega\mu_0 \left[\boldsymbol{J} + \frac{1}{k_0^2}\nabla(\boldsymbol{\nabla}\cdot\boldsymbol{J})\right], \tag{3}$$

$$\boldsymbol{\nabla}\cdot\boldsymbol{E}' = \frac{{\rm i}\omega\mu_0}{k_0^2}\boldsymbol{\nabla}\cdot\boldsymbol{J}, \tag{4}$$

where $k_0^2 = \omega^2\mu_0\varepsilon_0$ and $\boldsymbol{J} = I/c\delta(\rho-c)\delta(\varphi)\boldsymbol{e}_z$. The magnetic induction strength is $\boldsymbol{B}' = -(\boldsymbol{\nabla}\times\boldsymbol{E}')/({\rm i}\omega)$ and the magnetic field strength is $\boldsymbol{H}' = \boldsymbol{B}'/\mu_0$. $\boldsymbol{E}'$ can be divided into the incident field $\boldsymbol{E}'_{\rm in}$ caused only by the axial current and the scattering field $\boldsymbol{E}'_{\rm sc}$ caused only by the source equivalent to the cylindrical shell, $\boldsymbol{E}' = \boldsymbol{E}'_{\rm in} + \boldsymbol{E}'_{\rm sc}$. Their constraint equations are

$$\nabla^2 \boldsymbol{E}'_{\rm in} + k_0^2 \boldsymbol{E}'_{\rm in} = {\rm i}\omega\mu_0 \left[\boldsymbol{J} + \frac{1}{k_0^2}\nabla(\boldsymbol{\nabla}\cdot\boldsymbol{J})\right], \tag{5}$$

$$\boldsymbol{\nabla}\cdot\boldsymbol{E}'_{\rm in} = \frac{{\rm i}\omega\mu_0}{k_0^2}\boldsymbol{\nabla}\cdot\boldsymbol{J}, \tag{6}$$

and

$$\nabla^2 \boldsymbol{E}'_{\rm sc} + k^2 \boldsymbol{E}'_{\rm sc} = 0, \tag{7}$$

$$\boldsymbol{\nabla}\cdot\boldsymbol{E}'_{\rm sc} = 0. \tag{8}$$

2.2. Boundary conditions

The field region in $-h < z < h$ is divided into three sub-regions: V_1 $(0 < \rho \le a)$ and the fields are $\boldsymbol{E}_1$ and $\boldsymbol{H}_1$; $V_2 : a < \rho \le b$ and the fields are $\boldsymbol{E}$ and $\boldsymbol{H}$; $V_3 : b < \rho < +\infty$ and the fields are $\boldsymbol{E}_3$ and $\boldsymbol{H}_3$.

On the interface $\rho = a$, the boundary conditions are $E_{1\phi}(a,\phi,z) = E_\phi(a,\phi,z)$, $E_{1z}(a,\phi,z) = E_z(a,\phi,z)$, $H_{1\phi}(a,\phi,z) = H_\phi(a,\phi,z)$ and $H_{1z}(a,\phi,z) = H_z(a,\phi,z)$.

On the interface $\rho = b$, the boundary conditions are $E_\phi(b,\phi,z) = E_{3\phi}(b,\phi,z)$, $E_z(b,\phi,z) = E_{3z}(b,\phi,z)$, $H_\phi(b,\phi,z) = H_{3\phi}(b,\phi,z)$ and $H_z(b,\phi,z) = H_{3z}(b,\phi,z)$.

On both sides of the interface between the cylindrical shell and the air, $E_z = [{\rm i}\omega\varepsilon_0/(\gamma + {\rm i}\omega\varepsilon)]E'_z$. If the cylindrical shell is made of good conductive material and the frequency of the current is not very high, then $|{\rm i}\omega\varepsilon_0/(\gamma + {\rm i}\omega\varepsilon)| \approx \omega\varepsilon_0/\gamma$, which results in $E_z \approx 0$. For example, when $f = 1$ MHz and $\gamma = 10^4$ S/m, $\omega\varepsilon_0/\gamma \approx 10^{-8}$; $f = 1$ MHz and $\gamma = 10^6$ S/m, $\omega\varepsilon_0/\gamma \approx 10^{-10}$. Therefore, near two ends of the cylindrical shell, the boundary conditions are

$$E_z(\rho,\phi,h-0), \approx 0,$$

and

$$E_z(\rho,\phi,-h+0) \approx 0. \tag{9}$$

2.3. Analytical solutions

The field in V_2 and the scattering fields in V_1 and V_3 satisfy the homogeneous equations and can be easily solved out by the separation variable approach. The incident fields in V_1 and V_3 satisfy the inhomogeneous equations and can be solved out by a method similar to that in Refs. [6] and [15]. After the general solutions in each region are obtained, the boundary conditions are used to determine the undetermined constants. Finally, the analytical solutions to the fields in the cylindrical shell can be obtained

$$
\begin{aligned}
E_\rho &= \sum_{m=0}^{\infty}\sum_{n=0}^{\infty}\left\{-\frac{1}{s}a_{1n}\mathrm{J}_n'(\rho s)-\frac{1}{s}b_{2n}\left[\mathrm{H}_n^{(2)}(\rho s)\right]'+\frac{2}{\rho}c_{2n}\mathrm{J}_n(\rho s)+\frac{2}{\rho}d_{2n}\mathrm{H}_n^{(2)}(\rho s)\right\}\lambda_m\cos(n\phi)\sin(\lambda_m z),\\
E_\phi &= \sum_{m=0}^{\infty}\sum_{n=0}^{\infty}\left\{\frac{n}{\rho s^2}a_{2n}\mathrm{J}_n(\rho s)+\frac{n}{\rho s^2}b_{2n}\mathrm{H}_n^{(2)}(\rho s)-\frac{2s}{n}c_{2n}\mathrm{J}_n'(\rho s)-\frac{2s}{n}d_{2n}\left[\mathrm{H}_n^{(2)}(\rho s)\right]'\right\}\\
&\quad\times\lambda_m\sin(n\phi)\sin(\lambda_m z),\\
E_z &= \sum_{m=0}^{\infty}\sum_{m=0}^{\infty}[a_{2n}\mathrm{J}_n(\rho s)+b_{2n}\mathrm{H}_n^{(2)}(\rho s)]\cos(n\phi)\cos(\lambda_m z),
\end{aligned}
\tag{10}
$$

and

$$
\begin{aligned}
B_\rho &= \frac{1}{\mathrm{i}\omega}\sum_{m=0}^{\infty}\sum_{n=0}^{\infty}\left\{\frac{nk^2}{\rho s^2}a_{2n}\mathrm{J}_n(\rho s)+\frac{nk^2}{\rho s^2}b_{2n}\mathrm{H}_n^{(2)}(\rho s)-\frac{2\lambda_m^2 s}{n}c_{2n}\mathrm{J}_n'(\rho s)-\frac{2\lambda_m^2 s}{n}d_{2n}\left[\mathrm{H}_n^{(2)}(\rho s)\right]'\right\}\\
&\quad\times\sin(n\phi)\cos(\lambda_m z),\\
B_\phi &= -\frac{1}{\mathrm{i}\omega}\sum_{m=0}^{\infty}\sum_{n=0}^{\infty}\left\{-\frac{k^2}{s}a_{2n}\mathrm{J}_n'(\rho s)-\frac{k^2}{s}b_{2n}\left[\mathrm{H}_n^{(2)}(\rho s)\right]'+\frac{2\lambda_m^2}{\rho}c_{2n}\mathrm{J}_n(\rho s)+\frac{2\lambda_m^2}{\rho}d_{2n}\mathrm{H}_n^{(2)}(\rho s)\right\}\\
&\quad\times\cos(n\phi)\cos(\lambda_m z),\\
B_z &= -\frac{1}{\mathrm{i}\omega}\sum_{m=0}^{\infty}\sum_{n=0}^{\infty}\frac{2\lambda_m s^2}{n}[c_{2n}\mathrm{J}_n(\rho s)+d_{2n}\mathrm{H}_n^{(2)}(\rho s)]\sin(n\phi)\sin(\lambda_m z),
\end{aligned}
\tag{11}
$$

where $s=\sqrt{k^2-\lambda_m^2}$, λ_m is the separation constant and $\lambda_m=\pi(m+0.5)/h$; J_n and J_n' are the first type Bessel function of n-order and its partial derivative; $\mathrm{H}_n^{(2)}$ and $[\mathrm{H}_n^{(2)}]'$ are the third type Bessel function of n-order and its partial derivative. If $n=0$, then $c_{20}=0$, $d_{20}=0$, a_{20} and b_{20} can be solved by

$$
\boldsymbol{\alpha}\boldsymbol{X}=\boldsymbol{C},
\tag{12}
$$

where

$$
\boldsymbol{\alpha}=\begin{bmatrix}
\mathrm{J}_n(as_0) & -\mathrm{J}_n(as) & -\mathrm{H}_n^{(2)}(as) & 0\\
\dfrac{k_0^2}{s_0}\mathrm{J}_n'(as_0) & \dfrac{k^2}{\mu_\mathrm{r}s}\mathrm{J}_n'(as) & \dfrac{k^2}{\mu_\mathrm{r}s}\left[\mathrm{H}_n^{(2)}(as)\right]' & 0\\
0 & \mathrm{J}_n(bs) & \mathrm{H}_n^{(2)}(bs) & -\mathrm{H}_n^{(2)}(bs_0)\\
0 & -\dfrac{k^2}{\mu_\mathrm{r}s}\mathrm{J}_n'(bs) & -\dfrac{k^2}{\mu_\mathrm{r}s}\left[\mathrm{H}_n^{(2)}(bs)\right]' & \dfrac{k_0^2}{s_0}\left[\mathrm{H}_n^{(2)}(bs_0)\right]'
\end{bmatrix},
$$

$$
\boldsymbol{X}=\begin{bmatrix}a_{10} & a_{20} & b_{20} & b_{30}\end{bmatrix}^{\mathrm{T}},\quad \boldsymbol{C}=\begin{bmatrix}f_m\ln\dfrac{2}{k_0c} & 0 & -f_m\ln\dfrac{2}{k_0c} & 0\end{bmatrix}^{\mathrm{T}}
$$

and

$$
f_m=(-1)^m\frac{\mathrm{i}4\pi f\mu_0 I}{(2m+1)\pi^2}.
$$

If $n\geq 1$, a_{2n}, b_{2n}, c_{2n} and d_{2n} can be solved by

$$
\boldsymbol{\beta}\boldsymbol{Y}=\boldsymbol{D},
\tag{13}
$$

where

$\boldsymbol{\beta}$

$$
= \begin{bmatrix}
\frac{n}{as_0^2}\mathrm{J}_n(as_0) & -\frac{2s_0}{n}\mathrm{J}'_n(as_0) & -\frac{n}{as^2}\mathrm{J}_n(as) & -\frac{n}{as^2}\mathrm{H}_n^{(2)}(as) & -\frac{2s}{n}\mathrm{J}'_n(as) & \frac{2s}{n}\left[\mathrm{H}_n^{(2)}(as)\right]' & 0 & 0 \\
\mathrm{J}_n(as_0) & 0 & -\mathrm{J}_n(as) & -\mathrm{H}_n^{(2)}(as) & 0 & 0 & 0 & 0 \\
\frac{k_0^2}{s_0}\mathrm{J}'_n(as_0) & \frac{2\lambda_m^2}{a}\mathrm{J}_n(as_0) & \frac{k^2}{\mu_{\mathrm{r}}s}\mathrm{J}'_n(as) & \frac{k^2}{\mu_{\mathrm{r}}s}\left[\mathrm{H}_n^{(2)}(as)\right]' & -\frac{2\lambda_m^2}{a\mu_{\mathrm{r}}}\mathrm{J}_n(as) & -\frac{2\lambda_m^2}{a\mu_{\mathrm{r}}}\mathrm{H}_n^{(2)}(as) & 0 & 0 \\
0 & s_0^2\mathrm{J}_n(as_0) & 0 & 0 & -\frac{s^2}{\mu_{\mathrm{r}}}\mathrm{J}_n(as) & -\frac{s^2}{\mu_{\mathrm{r}}}\mathrm{H}_n^{(2)}(as) & 0 & 0 \\
0 & 0 & \frac{n}{bs^2}\mathrm{J}_n(bs) & \frac{n}{bs^2}\mathrm{H}_n^{(2)}(bs) & -\frac{2s}{n}\mathrm{J}'_n(bs) & -\frac{2s}{n}\left[\mathrm{H}_n^{(2)}(bs)\right]' & -\frac{n}{bs_0^2}\mathrm{H}_n^{(2)}(bs_0) & \frac{2s_0}{n}\left[\mathrm{H}_n^{(2)}(bs_0)\right]' \\
0 & 0 & \mathrm{J}_n(bs) & \mathrm{H}_n^{(2)}(bs) & 0 & 0 & -\mathrm{H}_n^{(2)}(bs_0) & 0 \\
0 & 0 & -\frac{k^2}{\mu_{\mathrm{r}}s}\mathrm{J}'_n(bs) & -\frac{k^2}{\mu_{\mathrm{r}}s}\left[\mathrm{H}_n^{(2)}(bs)\right]' & \frac{2\lambda_m^2}{b\mu_{\mathrm{r}}}\mathrm{J}_n(bs) & \frac{2\lambda_m^2}{b\mu_{\mathrm{r}}}\mathrm{H}_n^{(2)}(bs) & \frac{k_0^2}{s_0}\left[\mathrm{H}_n^{(2)}(bs_0)\right]' & -\frac{2\lambda_m^2}{b}\mathrm{H}_n^{(2)}(bs_0) \\
0 & 0 & 0 & 0 & \frac{s^2}{\mu_{\mathrm{r}}}\mathrm{J}_n(bs) & \frac{s^2}{\mu_{\mathrm{r}}}\mathrm{H}_n^{(2)}(bs) & 0 & -s_0^2\mathrm{H}_n^{(2)}(bs_0)
\end{bmatrix},
$$

$$
\boldsymbol{Y} = \begin{bmatrix} a_{1n} & c_{1n} & a_{2n} & b_{2n} & c_{2n} & d_{2n} & b_{3n} & d_{3n} \end{bmatrix}^{\mathrm{T}}
$$

and

$$
\boldsymbol{D} = \begin{bmatrix} 0 & \frac{f_m}{n}\left(\frac{a}{c}\right)^n & -\frac{f_m}{a}\left(\frac{a}{c}\right)^n & 0 & 0 & -\frac{f_m}{n}\left(\frac{b}{c}\right)^n & \frac{f_m}{b}\left(\frac{b}{c}\right)^n & 0 \end{bmatrix}^{\mathrm{T}}.
$$

3. Simplified solutions

For the cylindrical shells made of Fe-based amorphous material, nano-crystalline material and silicon steel material, μ_{r} and γ may be larger than 10^3 S/m and 10^6 S/m, and then $\mathrm{Im}(\rho s)$ becomes larger with the increase of f. Moreover, if the cylindrical shell is flat, which indicates a/h is large, then $\mathrm{Im}(\rho s_0)$ is large. For these cases, it is difficult to calculate out the numerical results of J_n, J'_n, $\mathrm{H}_n^{(2)}$ and $[\mathrm{H}_n^{(2)}]'$ by computers. Therefore, $\boldsymbol{\alpha}$ and $\boldsymbol{\beta}$ are close to being singular or badly scaled. Equations (12) and (13) cannot be fast and accurately solved out.

According to the asymptotic formulas of Bessel functions, when $|x| \to +\infty$ and $|\arg(x)| < \pi$, $\mathrm{J}_n(x) = \sqrt{2/\pi x}\cos(x - n\pi/2 - \pi/4)$, $\mathrm{J}'_n(x) = -\sqrt{2/\pi x}\sin(x - n\pi/2 - \pi/4)$, $\mathrm{H}_n^{(2)}(x) = \sqrt{2/\pi x}\ \exp[-\mathrm{i}(x - n\pi/2 - \pi/4)]$ and $\left[\mathrm{H}_n^{(2)}(x)\right]' = -\mathrm{i}\sqrt{2/\pi x}\ \exp[-\mathrm{i}(x - n\pi/2 - \pi/4)]$. Substituting these formulas into Eq. (12), a_{20} and b_{20} can be solved out

$$
a_{20} \approx -\frac{\mu_{\mathrm{r}}sk_0^2 f_m}{\mu_{\mathrm{r}}sk_0^2 - s_0k^2}\frac{1}{\mathrm{J}_n(bs)}\ln\left(\frac{2}{k_0c}\right), \quad b_{20} \approx \frac{\mu_{\mathrm{r}}sk_0^2 f_m}{\mu_{\mathrm{r}}sk_0^2 + s_0k^2}\frac{1}{\mathrm{J}_n(bs)}\ln\left(\frac{2}{k_0c}\right). \tag{14}
$$

Similarly, a_{2n}, b_{2n}, c_{2n} and d_{2n} $(n \geq 1)$ can be solved out

$$
\begin{aligned}
a_{2n} &\approx -\frac{(u_{45}u_{77} - u_{45}u_{78} - u_{42}u_{77} + u_{42}u_{75})D_6 + (u_{42}u_{67} - u_{45}u_{67})D_7}{(u_{45}u_{77} - u_{45}u_{78} - u_{42}u_{77} + u_{42}u_{75})(u_{67} - u_{63}) + (u_{42}u_{67} - u_{45}u_{67})(u_{77} + u_{73})}\frac{1}{\beta_{53}}, \\
b_{2n} &\approx -\frac{(u_{45}u_{32} - u_{45}u_{31} - u_{42}u_{71} - u_{42}u_{35})D_2 + (u_{21}u_{42} - u_{45}u_{21})D_3}{(u_{45}u_{32} - u_{45}u_{31} - u_{42}u_{71} - u_{42}u_{35})(u_{21} - u_{23}) - (u_{21}u_{42} - u_{45}u_{21})(u_{33} - u_{31})}\frac{1}{\beta_{14}}, \\
c_{2n} &\approx \frac{-u_{42}(u_{77} + u_{73})D_6 + u_{42}(u_{67} - u_{63})D_7}{(u_{45}u_{77} - u_{45}u_{78} - u_{42}u_{77} + u_{42}u_{75})(u_{67} - u_{63}) + (u_{42}u_{67} - u_{45}u_{67})(u_{77} + u_{73})}\frac{1}{\beta_{55}}, \\
d_{2n} &\approx \frac{u_{42}(u_{33} - u_{31})D_2 + u_{42}(u_{21} - u_{23})D_3}{(u_{45}u_{32} - u_{45}u_{31} - u_{42}u_{71} - u_{42}u_{35})(u_{21} - u_{23}) - (u_{21}u_{42} - u_{45}u_{21})(u_{33} - u_{31})}\frac{1}{\beta_{16}},
\end{aligned} \tag{15}
$$

where $\beta_{53}, \beta_{14}, \beta_{55}$ and β_{16} are elements of $\boldsymbol{\beta}$; D_2, D_3, D_6 and D_7 are elements of $\boldsymbol{D}$; u_{ij} $(i = 1, \ldots, 8; j =$

$1,\ldots,8$) are elements of the following matrix

$$\boldsymbol{u}=\begin{bmatrix} 1 & 1 & 1 & 1 & 1 & 1 & 0 & 0 \\ \frac{as_0^2}{n} & 0 & \frac{as^2}{n} & \frac{as^2}{n} & 0 & 0 & 0 & 0 \\ \mathrm{i}\frac{k_0^2as_0}{n} & \mathrm{i}\frac{n\lambda_m^2}{as_0} & -\mathrm{i}\frac{k^2as}{n\mu_\mathrm{r}} & \frac{k^2as}{n\mu_\mathrm{r}} & \mathrm{i}\frac{n\lambda_m^2}{\mu_\mathrm{r}as} & -\mathrm{i}\frac{n\lambda_m^2}{\mu_\mathrm{r}as} & 0 & 0 \\ 0 & -\mathrm{i}\frac{ns_0}{2} & 0 & 0 & \mathrm{i}\frac{ns}{2\mu_\mathrm{r}} & -\mathrm{i}\frac{ns}{2\mu_\mathrm{r}} & 0 & 0 \\ 0 & 0 & 1 & 1 & 1 & 1 & 1 & 1 \\ 0 & 0 & \frac{bs^2}{n} & \frac{bs^2}{n} & 0 & 0 & \frac{bs_0^2}{n} & 0 \\ 0 & 0 & -\mathrm{i}\frac{k^2bs}{n\mu_\mathrm{r}} & \mathrm{i}\frac{k^2bs}{n\mu_\mathrm{r}} & \mathrm{i}\frac{n\lambda_m^2}{\mu_\mathrm{r}bs} & -\mathrm{i}\frac{n\lambda_m^2}{\mu_\mathrm{r}bs} & \mathrm{i}\frac{k_0^2bs_0}{n} & -\mathrm{i}\frac{n\lambda_m^2}{bs_0} \\ 0 & 0 & 0 & 0 & \mathrm{i}\frac{ns}{2\mu_\mathrm{r}}\beta_{55} & -\mathrm{i}\frac{ns}{2\mu_\mathrm{r}} & 0 & -\mathrm{i}\frac{ns_0}{2} \end{bmatrix}.$$

Letting $\varsigma=\sqrt{b/\rho}\,\mathrm{e}^{\,\mathrm{i}(\rho-b)s}$ and $\xi=\sqrt{a/\rho}\,\mathrm{e}^{\,\mathrm{i}(a-\rho)s}$, the simplified solutions to the electromagnetic field in the cylindrical shell are expressed as

$$\begin{aligned} E_\rho &= -\mathrm{i}\sum_{m=0}^{\infty}\left[\frac{1}{s}\left(q_1\varsigma+q_2\xi\right)\right]\lambda_m\sin\left(\lambda_m z\right)+\sum_{m=0}^{\infty}\sum_{n=1}^{\infty}\left[\mathrm{i}\left(\frac{n}{\rho s}Q_3-\frac{s}{n}bQ_1\right)\varsigma+\left(\frac{n}{\rho s}Q_4-\frac{s}{n}aQ_2\right)\xi\right] \\ &\quad\times\lambda_m\cos\left(n\phi\right)\sin\left(\lambda_m z\right), \\ E_\phi &= \sum_{m=0}^{\infty}\sum_{n=1}^{\infty}\left[\left(\frac{1}{\rho}Q_1b+Q_3\right)\varsigma-\left(\frac{1}{\rho}Q_2a+Q_4\right)\xi\right]\lambda_m\sin\left(n\phi\right)\sin\left(\lambda_m z\right), \\ E_z &= \sum_{m=0}^{\infty}\left(q_1\varsigma-q_2\xi\right)\cos\left(\lambda_m z\right)+\sum_{m=0}^{\infty}\sum_{n=1}^{\infty}\frac{s^2}{n}\left(Q_1b\varsigma-Q_2a\xi\right)\cos\left(n\phi\right)\cos\left(\lambda_m z\right), \end{aligned} \tag{16}$$

and

$$\begin{aligned} B_\rho &= \frac{1}{\mathrm{i}\omega}\sum_{m=0}^{\infty}\sum_{n=1}^{\infty}\left[\left(\frac{k^2}{\rho}Q_1b+\lambda_m^2Q_3\right)\varsigma-\left(\frac{k^2}{\rho}Q_2a+\lambda_m^2Q_4\right)\xi\right]\sin\left(n\phi\right)\cos\left(\lambda_m z\right), \\ B_\phi &= \frac{k^2}{\omega s}\sum_{m=0}^{\infty}\left(q_1\varsigma+q_2\xi\right)\cos\left(\lambda_m z\right)+\frac{1}{\omega}\sum_{m=0}^{\infty}\sum_{n=1}^{\infty}\left[\left(\frac{k^2s}{n}Q_1b-\frac{\lambda_m^2n}{\rho s}Q_3\right)\varsigma+\left(\frac{k^2s}{n}Q_2a-\frac{\lambda_m^2n}{\rho s}Q_4\right)\xi\right] \\ &\quad\times\sin\left(n\phi\right)\cos\left(\lambda_m z\right), \\ B_z &= -\frac{1}{\omega}\sum_{m=0}^{\infty}\sum_{n=1}^{\infty}\lambda_m s\left[Q_3\varsigma+Q_4\xi\right]\sin\left(n\phi\right)\sin\left(\lambda_m z\right), \end{aligned} \tag{17}$$

Equations (16) and (17) do not contain Bessel functions. Because of $a\le\rho\le b$, ς and ξ should not be represented as conventional floating-point values.

4. Numerical analysis and experiments

4.1. Comparisons

It is noticeable that only one approximate boundary condition (Eq. (9)) is used in Section 2 and its error is very small (about $\le 10^{-8}$), so equations (10) and (11) can be thought as the accurate analytical solutions to the electromagnetic field in the ferrite shell. Equations (16) and (17) are the simplified approximate solutions. To validate these solutions some models are calculated.

Assume $\mu_\mathrm{r}=1000$, $\gamma=100$ S/m, $\varepsilon=8.85\times10^{-12}$ F/m, $\mu_0=4\pi\times10^{-7}$ H/m, $\varepsilon_0=8.85\times10^{-12}$ F/m, $I=1$ A, $a=0.5$ m, $b=0.6$ m, $c=0.8$ m and $h=0.03$ m. Equations (16) and (17) can be calculated out faster than Eqs. (10) and (11). Figures 2 and 3 show the distribution of $\boldsymbol{E}$ and $\boldsymbol{B}$ along the

circumference in the shell where $\rho = (a + b)/2$ and $z = 0.01$ m.

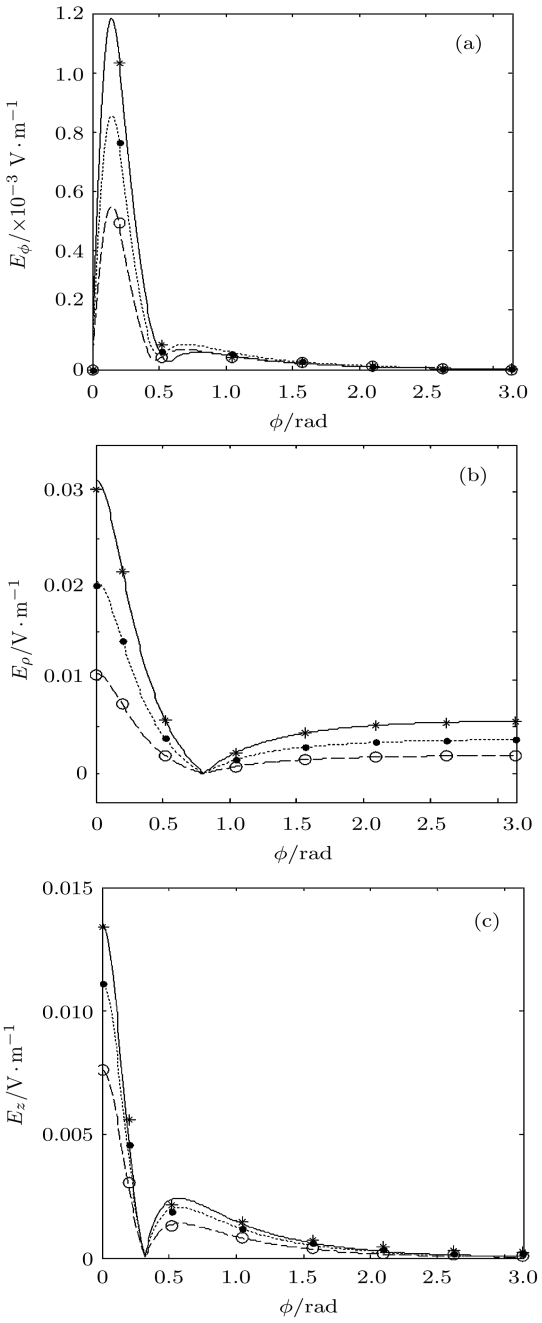


Fig. 2. (a) Distribution of E_ϕ. (b) Distribution of E_ρ. (c) Distribution of E_z. The solid lines, dot lines and dash lines corresponding to $f = 10$ kHz, $f = 5$ kHz and $f = 1$ kHz describe the results by Eqs. (14) and (15). The symols '$*$', '$\bullet$' and 'o' corresponding to $f = 10$ kHz, $f = 5$ kHz and $f = 1$ kHz are the results by Eqs. (8) and (9).

It can be found that the accuracy of the simplified solutions is close to the analytical ones. With the increase of frequency, $\boldsymbol{E}$ becomes stronger and $\boldsymbol{B}$ becomes weaker. From Fig. 2, $E_\rho > E_z > E_\phi$. Because the eddy current density in the shell is $\gamma\boldsymbol{E}$, the radial eddy current is largest. To reduce such eddy current loss, the cylindrical shells in high frequency applications should be made by winding the thin ferrite sheet.

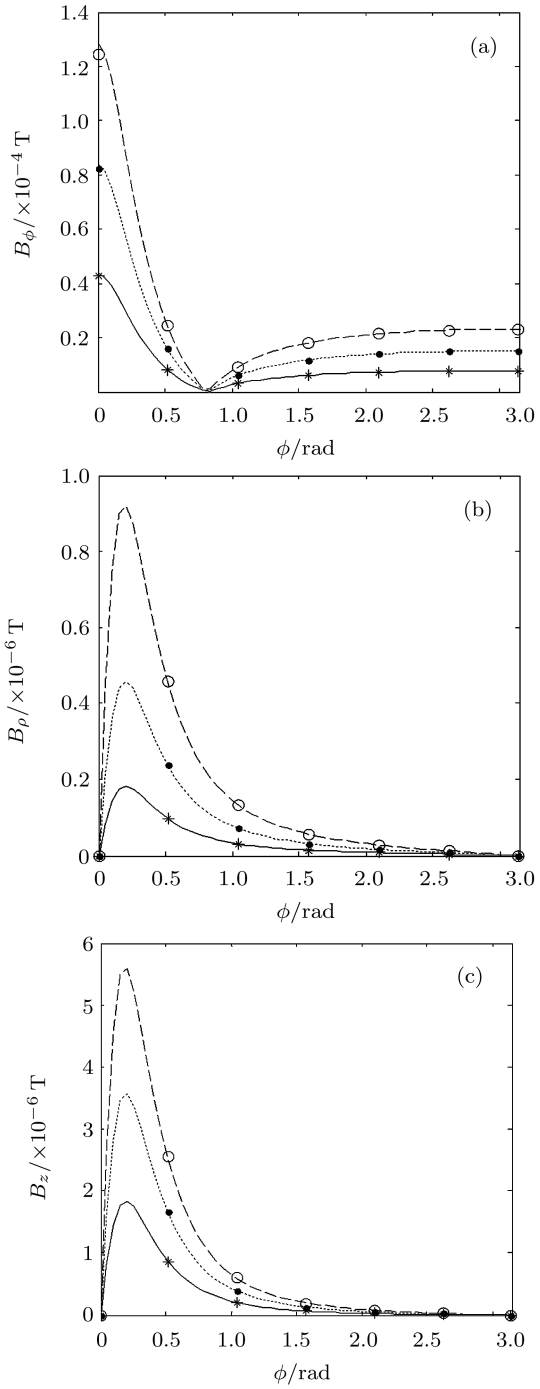


Fig. 3. (a) Distribution of B_ϕ. (b) Distribution of B_ρ. (c) Distribution of B_z. The solid lines, dot lines and dash lines corresponding to $f = 10$ kHz, $f = 5$ kHz and $f = 1$ kHz describe the results by Eqs. (14) and (15). The symbols '$*$', '$\bullet$' and 'o' respectively corresponding to $f = 10$ kHz, $f = 5$ kHz and $f = 1$ kHz are the results by Eqs. (8) and (9).

From Fig. 3, $B_\phi > B_z > B_\rho$. For many devices such as current transformers in electrical engineering, the external axial current may reach more than 100 kA

and the magnetic shell is easily saturated. Moreover, such interference will induce the additional voltage on the solenoid coils around the shell, which can reduce the accuracy of the devices. It is necessary to shield such magnetic field.

According to Eq. (15), the distribution of B_ϕ along the radius in the shell is shown in Fig. 4. B_ϕ varies with z. Close to the ending surface of the shell, B_ϕ becomes weak, and B_ϕ is strongest at $z = 0$. At the inner and outer cylindrical surface in the shell, especially at the outer cylindrical surface near the current, B_ϕ is strongest.

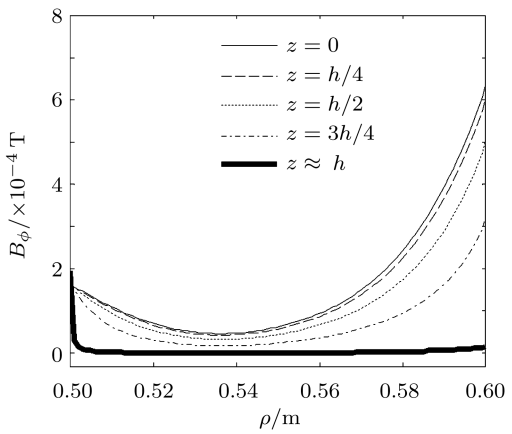


Fig. 4. Distribution of B_ϕ along the radius.

Additionally, when $\mu_r > 5000$, $\gamma > 1000$ S/m and $f > 1$ kHz, it is difficult to calculate out Eqs. (11) by computers because $\boldsymbol{\alpha}$ and $\boldsymbol{\beta}$ are very singular.

4.2. Measurements

To validate Eqs. (17), a cylindrical shell-shaped core made of Mn–Zn ferrite is wound tightly by coils A and B. Its parameters are $\mu_r = 1000$, $\gamma = 100$ S/m, $\varepsilon = 8.85 \times 10^{-12}$ F/m, $a = 0.013$ m, $b = 0.0225$ m and $h = 0.00388$ m. The angle covered by coil A is $\pi/6$ and by coil B is $5\pi/12$. The turn numbers of coils A and B are respectively 80 and 30.

The experimental schematic diagram is shown in Fig. 5. The axial current is generated by Fluke 5520 A calibrator, and its effective value is 1 A. Changing the frequency and the position of the current, the induction voltages at the coils are measured by Agilent 34401 A digital multi-meter, which can also be calculated by the following formula

$$U = \mathrm{i}\omega \int_{\phi_1}^{\phi_2} n_c \mathrm{d}\varphi \int_a^b \int_{-h}^{h} B_\phi \mathrm{d}\rho \mathrm{d}z, \qquad (18)$$

where n_c is the turn density and its unit is turns per rad; ϕ_1 and ϕ_2 are the initial and the end angles of the coils.

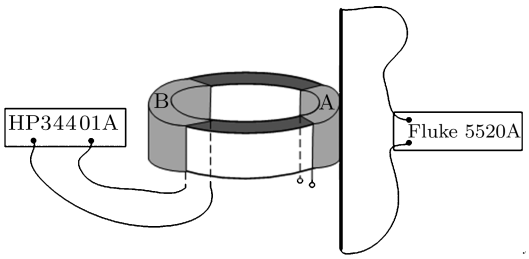


Fig. 5. Experimental schematic diagram.

When I is positioned at the outside and middle of coil A or coil B, the measured and calculated induction voltages are shown in Table 1. In despite of the non-uniformity of the coils, the magnetic field leakage, the inaccurate parameters of the shell, the measured results are close to the calculated results. The errors between them are small when the frequency is high.

Table 1. Comparison between the measured and calculated results. "Meas." represents the measured results and "Cal." represents the results calculated by Eq. (18).

f/kHz	$I = 1$ A outside of coil A				$I = 1$ A outside of coil B			
	coil A		coil B		coil A		coil B	
	Meas./mV	Cal./mV	Meas./mV	Cal./mV	Meas./mV	Cal./mV	Meas./mV	Cal./mV
1	2.22	0.79	1.78	2.57	1.35	0.82	4.25	6.79
5	7.12	5.37	14.53	12.42	4.25	3.95	34.51	34.37
10	14.56	15.47	21.74	22.69	7.33	7.27	72.40	70.51

5. Conclusions

Accurate analytical solutions to the electromagnetic field in the finite length cylindrical shaped ferrite shell excited by the external axial current have been derived. For the shell with high permeability and conductivity, simplified solutions to the high-frequency field have been obtained by using the asymptotic formulas of Bessel

functions. The simple solutions do not contain complex Bessel functions and the inverse operation of 4×4 and 8×8 matrixes. They can be calculated out fast by computers. Comparisons of the numerical results show that the accuracy of the simple solutions is close to that of the analytical solutions. The physical experiments also validate the simple solutions. The solutions obtained in this paper are convenient to calculate the field distribution and the eddy current losses in the cylindrical shell.

References

[1] Dodd C V and Deeds W E 1968 *J. Appl. Phys.* **39** 2829

[2] Zhao T E, Wu R X, Yang F and Chen P 2006 *Acta Phys. Sin.* **55** 179 (in Chinese)

[3] Jiao C Q and Luo J R 2006 *Acta Phys. Sin.* **55** 6360 (in Chinese)

[4] Hu S D, Li Z J and Zhang B 2009 *Chin. Phys.* B **18** 315

[5] Tegopoulos J A and Kriezis E E 1973 *IEEE Trans. Power Appl. Syst.* **92** 742

[6] Kriezis E E, Chrissoulidis D P and Georgiadis L G 1982 *IEE Proc. Part A* **129** 54

[7] Gong L, Hagel R, Zhang K and Unbehauen R 1992 *IEEE Trans. Magn.* **28** 1154

[8] Namjoshi K V, Lavers J D and Biringer P P 1998 *IEEE Trans. Magn.* **34** 636

[9] Namjoshi K V, Lavers J D and Biringer P P 1994 *IEEE Trans. Magn.* **30** 85

[10] Wu J and Lei Y Z 2002 *J. Phys.* D **35** 570

[11] Bowler N 2004 *J. Appl. Phys.* **95** 344

[12] Siva Kumar V, Kelekanjeri G and Gerhardt Rosario A 2007 *J. Appl. Phys.* **101** 044904

[13] Theodoulidis Theodoros P 2003 *J. Appl. Phys.* **95** 3071

[14] Theodoulidis Theodoros P 2008 *J. Appl. Phys.* **103** 024905

[15] Lei Y Z 2000 *Analysis Method on Time-harmonic Electromagnetic Fields* (Beijing: Science Press) p. 217